Journal of Electronic Materials, Vol. 22, No. 10, 1993

Special Issue Paper

Crystallization and Stability of the $Bi_2Sr_2CaCu_2O_x$ Superconductor

D.J. MILLER, T.G. HOLESINGER, J.L. ROUTBORT

Materials Science Division and Science and Technology Center for Superconductivity, Argonne National Laboratory, Argonne, IL 60439

K.C. GORETTA

Materials Components and Technology, Argonne National Laboratory, Argonne, IL 60439

L.S. CHUMBLEY

Department of Materials Science and Engineering, Iowa State University and Ames Laboratory, Ames, IA 50011

A basic study of the stability of the $Bi_2Sr_2CaCu_2O_x$ phase has been carried out in order to identify the composition and processing conditions for optimum superconducting properties. Analytical electron microscopy has been used to follow the crystallization of this phase during annealing in the solid state as well as from the melt. The crystal chemistry and phase purity is found to depend strongly on the processing conditions. Significant differences in crystallization behavior may be related to kinetic limitations of oxygen transport. The $Bi_2Sr_2CaCu_2O_x$ phase has also been subjected to thermomechanical processing in order to improve our understanding of the deformation processes involved during fabrication of wires and tapes. It has been found that mechanical deformation can have significant effects on the microstructure of the material which in turn result in changes in superconducting properties.

Key words: Analytical electron microsocpy, Bi-2212, critical current density, flux pinning, hot isostatic pressing, mechanical creep, melt processing, splat-quenched glass, oxygen partial pressure

INTRODUCTION

Significant attention is still being directed toward the Bi-Sr-Ca-Cu-O superconductors for a variety of applications. Common processing routes involve mechanical consolidation and sintering as used, for example, during powder-in-tube processing for wires and tapes, glass-ceramic processing, and melt casting. Knowledge of the phase evolution and properties of these Bi-Sr-Ca-Cu-O superconductors plays an important role in developing these processes to fabricate practical conductors and devices. Thus, an improved knowledge of the crystallization and deformation behavior is crucial in the further development of these materials.

The superconducting phases in this system are generally referred to by an ideal formula $Bi_2Sr_2Ca_{n-1}Cu_nO_y$, where n represents the number of CuO_2 planes. Thus, although each phase may exist over a wide range of compositions, the three well-known phases are commonly referred to as 2201, 2212, and 2223, with approximate transition temperatures of 10, 85, and 110K, respectively.[1,2] Although the Bi-2223 superconducting phase exhibits a high transition temperature, all of the double-layer Bi-based compounds are limited somewhat by their irreversibility behavior as a consequence of poor coupling between adjacent CuO_2 layers.[3] A number of applications have been proposed for the high temperature superconductors covering a range of current density and magnetic field requirements,[4] but the most advantageous operating temperature for these applications is at 77K, severely restricting the applicability of the Bi-based superconductors. Thus, the

(Received February 23, 1993)

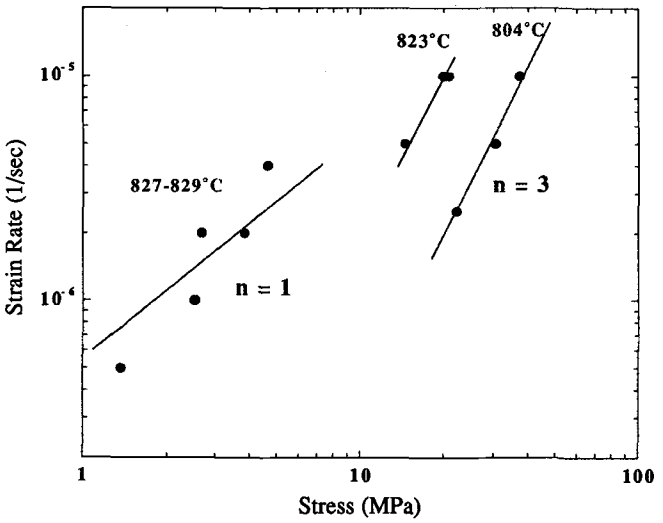

Fig. 1. Plot of the steady-state strain rate, $\dot{\varepsilon}$, against steady-state stress, σ, for samples subjected to creep deformation in the temperature range from ≈800 to 830°C.

Fig. 2. Bright field transmission electron micrograph of a sample compressed ≈750°C and ≈50 MPa (high stress regime) showing the dislocation structure associated with dislocation creep.

Bi-based superconductors are likely to be viable choices for use only in either high-temperature, low-field applications or low-temperature, high-field applications. Given these constraints, the 2212 phase is an attractive candidate for applications such as current leads, for example, which require high critical currents and low thermal dissipation, or superconducting magnets which would be operated in cryo-pumped systems.

Two convenient techniques for preparing bulk forms of Bi-2212 involve direct casting from the melt or glass-ceramic processing. Crystallization from the amorphous state has successfully been used for producing high-temperature superconducting phases in the Bi-Sr-Ca-Cu-O system in thin film, fiber, and bulk forms.[5–7] Conversion of these materials to a superconducting phase requires an understanding of the crystallization process in order to maximize the superconducting properties while controlling the microstructure and phase assemblage. Several groups have investigated various aspects of crystallization of the 2212 and 2223 phases from the amorphous state.[8–11] Most of these studies found the low-T_c phase (2201) to crystallize first. Oxygen deficiencies in these quenched glasses[12] are likely to affect phase formation since the superconducting phases are not observed to form in the absence of O_2. In this study, both short and extended anneals were employed to determine the crystallization process for glasses around the 2212 stoichiometry.

Another common process used to fabricate bulk components of Bi-2212 involves consolidation of powders. Combinations of rolling or pressing followed by thermal annealing are widely used during the fabrication of wires and tapes, while bulk components have been prepared by pressing and sintering, sinter-forging, or hot-isostatic pressing.[13–17] Thus, a knowledge of the high-temperature deformation behavior is of benefit in optimizing the time-temperature-stress processing conditions. In this work, the stress-strain behavior and deformation mechanisms during high-temperature creep were examined by mechanical testing and transmission electron microscopy.

EXPERIMENTAL

The starting material for most aspects of these studies consisted of Bi-2212 powders. The 2212 powder was synthesized by reaction of a mixture of Bi_2O_3, $SrCO_3$, $CaCO_3$, and CuO. The powders were calcined between 780–800°C for 30 h with an intermediate and final grinding. No $Bi_2Sr_2CuO_x$ (2201) phase was observed by x-ray diffraction, although it is likely that the powder contained a few percent of a mixture of the 2201 phase and residual Ca-Cu oxides. No low-melting-temperature phases were observed by differential thermal analysis (DTA) of the 2212 powder. Amorphous material was prepared by splat quenching. Reacted powders were placed in a metallurgical-grade alumina crucible and held for 45 min at 1075°C. The melt was then poured onto a stainless steel plate heated to 200°C and immediately quenched from above with a large Cu anvil.

For the mechanical deformation and consolidation studies, 2212 powders were processed into bulk forms by hot isostatic pressing (HIPing). The 2212 powder was cold-pressed at a pressure of 50 MPa, wrapped in Ag foil, sealed in an evacuated stainless steel can, and HIPed in an inert atmosphere at 825°C. The pressure of 105 MPa was applied for times ranging from 15 to 120 min. Large 3–4 mm thick discs were sliced, and several test specimens were cut from each with a slow-speed diamond-blade saw. The densities of the specimens, measured geometrically, were 6.6 g/cm^3. X-ray diffraction analyses determined that the specimens exhibited only modest texturing.[18]

Temperatures of thermal events for amorphous or annealed samples were determined by DTA using a Perkin Elmer 1700 system. Small amounts of freshly ground powder were cycled at a rate of 10°C/min in O_2 or Ar with a gas flow of 50 cc/min. Samples were

annealed in a sealed quartz tube furnace with oxygen or argon flow rates of 50 cc/min. Anneal times ranged from 1 min up to 1000 h at temperatures from 475 to 865°C. Superconducting properties were evaluated by standard four-probe resistivity measurements or magnetization measurements using a Quantum Design SQUID magnetometer.

Creep samples were compressed in air between Al_2O_3 platens at a constant crosshead velocity in a testing machine equipped with a high-temperature furnace and a muffle tube. The specimens were deformed until an apparent steady state was reached. For most specimens, $\dot{\varepsilon}$ or temperature was changed during the test and more than one apparent steady state was established.

In all cases, samples were prepared for transmission electron microscopy (TEM) using standard techniques. Pieces were sectioned by slicing with a low-speed diamond saw. The samples were then thinned by low-speed grinding followed by mechanical dimpling and polishing. The dimpled samples were ion milled to final perforation at liquid nitrogen temperature using a 4kV Ar beam. Transmission electron microscopy was performed in a Philips CM-30 operated at 100 kV.

RESULTS AND DISCUSSION

The mechanical creep tests were carried out at temperatures ranging from 750 to ≈830°C. The data from several samples tested in approximately the same temperature range are shown in Fig. 1 in which the steady-state strain rate, $\dot{\varepsilon}$, is plotted against steady-state stress, σ. In the generalized creep equation, $\dot{\varepsilon} \propto \sigma^n$. From the data, it is apparent that there are two creep regimes, one at lower stresses in which the stress exponent is near unity[19] while at higher stresses the stress exponent ≈3. These data suggest a change in deformation mechanisms from one dominated by diffusional flow at low stresses to one dominated by dislocation creep at higher stresses. Microstructural characterization of the creep samples has been carried out by TEM, and an example of the microstructure of a sample deformed in the high-stress regime is shown in Fig. 2. In this figure, extended dislocations separated by stacking faults are visible, confirming the occurrence of dislocation glide during deformation. Although the presence of these crystal defects suggests that it may be possible to form these materials by mechanical deformation, the strain rates are very low. Large strains result in microcracking due to a limited number of low-energy slip systems in 2212. Magnetization measurements on compressed and uncompressed samples show approximately a factor of two increase a magnetic hysteresis for the compressed samples, indicating that these defects are effective in pinning flux.

These results suggest that low-strain deformation during processing may be used to introduce defects which will enhance flux pinning. However, this enhanced magnetization is reduced at temperatures above ≈20K due to the two-dimensional nature of 2212 at those temperatures.

The creep behavior of 2212 is expected to become important during consolidation by HIPing. In order to examine the consolidation mechanisms, samples were HIPed at 825°C and 105 MPa for times ranging from 12 to 120 min. As shown in Fig. 3 and confirmed by density measurements, samples HIPed for 15 min had attained a density ≥99% of theoretical. In addition, most of the grains contain a high dislocation density, suggesting that consolidation occurs by dislocation creep as well as particle fragmentation and rearrangement. Hot isostatic pressing for longer times results in the annihilation of these defects however, since under the nearly hydrostatic stress conditions of HIP, once the sample reaches full density, most of the mechanisms for new dislocation generation are eliminated and recovery processes can dominate. This is illustrated in Fig. 4 which shows the microstructure of a sample HIPed for 45 min. In this image, low-angle grain boundaries are visible within the bent grain as dislocations of like sign glide toward

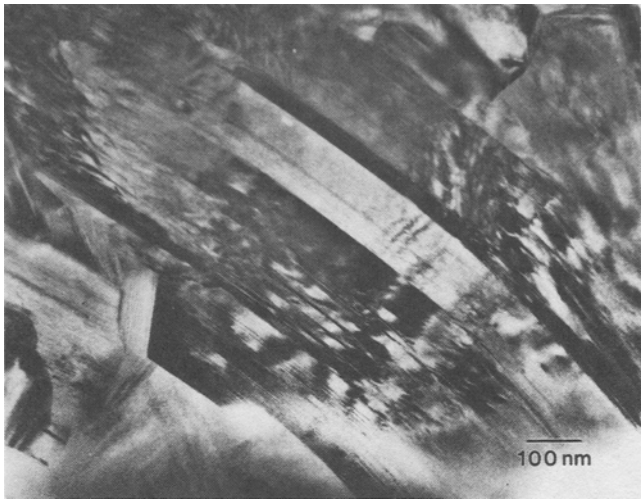

Fig. 3. Bright field transmission electron micrograph of a sample consolidated by HIP at 825°C and 105 MPa for 15 min.

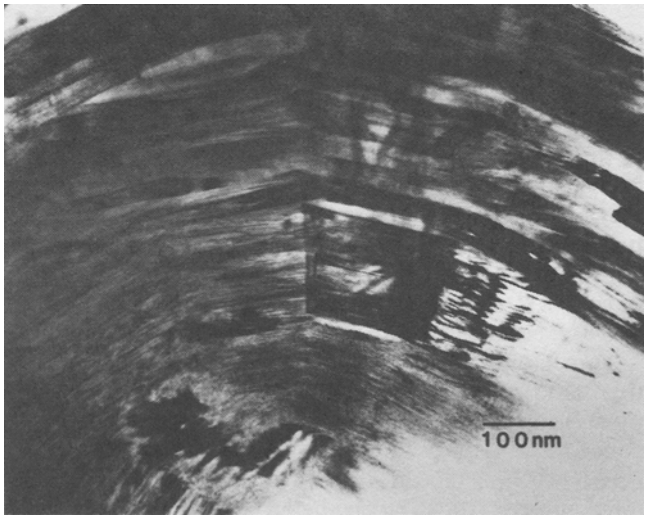

Fig. 4. Bright field transmission electron micrograph of a sample consolidated by HIP at 825°C and 105 MPa for 45 min.

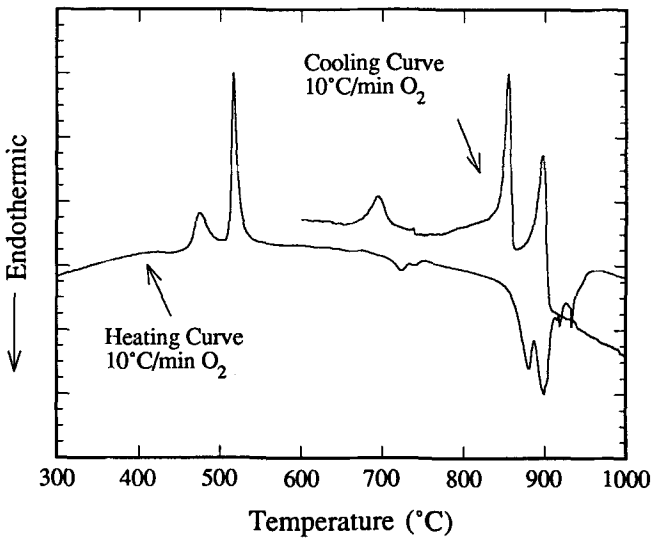

Fig. 5. Differential thermal analysis scans of Bi-2212 for both heating and cooling at 10°C/min in 100% oxygen.

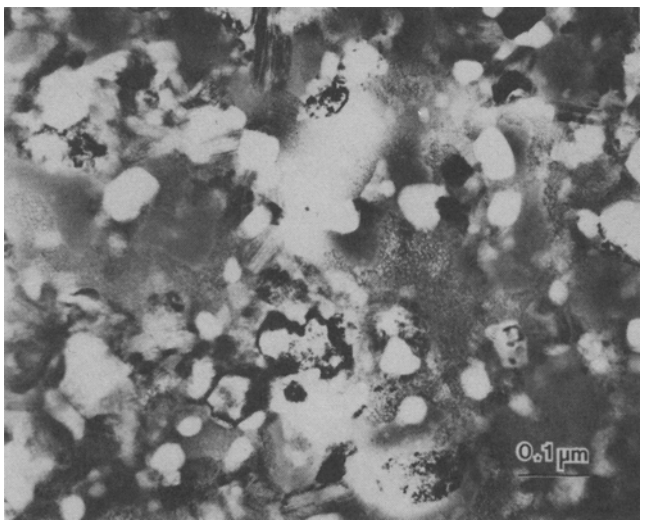

Fig. 6. Bright field transmission electron micrograph of a splat-quenched sample annealed at 650°C for 1 min.

one another to minimize the interaction energy of their strain fields. After further HIPing up to 120 min, recovery is more fully complete and far fewer dislocations are visible within the 2212 grains. As in the case of material which has undergone mechanical creep, these defects are expected to contribute to enhanced flux pinning, and this behavior has been confirmed by magnetization data, the samples HIPed for 15 min exhibiting expanded magnetization hysteresis compared to those HIPed for 120 min for which many of the defects are annihilated.[20]

The formation of the Bi-2212 phase was studied during crystallization of amorphous glass as well as by solidification from the melt. In each case, oxygen was found to play an important role in the development of phases. Amorphous glass was prepared by splat quenching as described above. The amorphous structure of the glass was confirmed by x-ray diffraction (XRD), scanning electron microscopy (SEM), and TEM. Differential thermal analysis was used to identify the thermal events associated with crystallization, and heating and cooling curves are shown in Fig. 5. In this plot, several thermal events associated with crystallization are visible in the heating curve. Two crystallization exotherms are apparent at low temperatures, one near 460°C, the other near 500°C. Around 700°C a small endotherm is visible, while two strong endotherms occur above 850°C. In order to identify the crystallization events associated with each peak, samples were annealed for 1 min at temperatures just below and just above the peaks and then characterized by XRD and TEM. For samples annealed at 475°C, the XRD spectrum shows only a broad amorphous peak typical of the splat-quenched glass. However, examination by TEM revealed the presence of many small crystallites which were identified from lattice fringe spacings as the 2201 phase.[21] Likewise, samples annealed at 500°C exhibited a microcrystalline structure consisting primarily of 2201 and CuO, suggesting that the first small exotherm ≈475°C corresponds to the initial nucleation of 2201. Samples annealed at 550 or 650°C, above the second strong exotherm near 500°C, show a polycrystalline structure consisting of $Bi_2Sr_{3-x}Ca_xO_y$ (23X), SrO, CaO, and Cu_2O, as shown, for example, in Fig. 6 for the sample annealed at 650°C. Annealing for long times at these temperatures, up to 1000 h, results in the gradual conversion of the 23X phase to 2201 and 2212. These results indicate that the second strong exotherm corresponds to the crystallization of 23X, SrO, CaO, and Cu_2O in an oxygen deficient environment. As noted previously, the splat-quenched glasses are deficient in oxygen and, at these low temperatures, the diffusion of oxygen into the sample is kinetically limited.[22] Thus, the initial crystallization of 2201 consumes most of the oxygen available in the glass while the remaining glass must crystallize into phases associated with an oxygen deficiency. Thus, the final conversion to 2212 is limited by the kinetics of oxygen diffusion in the solid state. There is a marked difference in microstructure for samples annealed above the endotherm at 700°C, however, as shown in Fig. 7 for a sample annealed at 750°C. At this temperature, the conversion to 2212 is essentially complete within the 1 min annealing time. Based upon DTA analysis of samples annealed in Ar, it is concluded that some melting of the oxygen deficient phases occurs at these temperatures. The presence of this liquid promotes diffusion of both cations as well as oxygen, resulting in rapid growth of the 2212 phase. The microstructures of samples annealed at higher temperatures, up to 865°C, do not differ significantly. Significant differences in the resistivity of samples annealed for longer times are observed, however, as shown in Fig. 8. Comparison the normalized resistivity for the samples annealed at 865°C shows a progressively sharper transition with increased annealing time. In particular, the resistive tail which significantly reduces $T_{c,R=0}$ and is generally associated with poorly coupled grain boundaries is minimized with increased an-

nealing time. Also plotted in Fig. 8 is the R vs T curve for a sample annealed at 875°C, just above the temperature for the onset of melting. The sharp transition and high zero resistance temperature indicate the benefit of some melting in terms of improving grain boundary coupling.

Improvements in properties associated with melt processing, such as the resistivity behavior noted above, underscore the importance of developing a good understanding of the solidification process. In this work, the microstructure of samples solidified under various oxygen partial pressures were examined and correlated with DTA data in order to identify the solidification sequence. As shown in Fig. 5, several exothermic peaks are visible in the cooling curve for samples solidified in oxygen, corresponding to crystallization of various phases. The curve shown is for solidification in 100% oxygen. Qualitatively, curves for samples solidified in reduced oxygen pressures are similar, but the onset temperatures for the higher-temperature exotherms decrease with decreasing oxygen pressure. During solidification in argon, only a single high-temperature exotherm is observed while the lower temperature peak, with an onset near 750°C, remains constant for all samples. The microstructures of solidified samples were examined by SEM, and an example of the microstructure of a sample solidified in an argon atmosphere is shown in Fig. 9. Three distinct constituents are visible in the micrograph. The larger dark particles are CaO, which precipitates in the melt and is difficult to avoid during melt processing. The other constituents correspond to the two crystallization exotherms noted. Primary crystallization of the large, blocky particles of the 23X phase is followed by eutectic solidification of a mixture of 23X, Cu_2O, and a small amount of 2201. These are the same phases observed to form during crystallization of the splat-quenched glass under an oxygen deficiency. Solidification under increasing oxygen partial pressures results in a change in the primary solidification products. As shown in Fig. 10 for a sample solidified under 100% oxygen, primary crystallization of Cu-rich phases, which are visible as large dark particles, takes place followed by nucleation of 2212 and 2201 platelets. Solidification is completed by solidification of the same eutectic mixture observed during solidification in an argon atmosphere. Small regions of this eutectic are visible between the 2212/2201 platelets. Thus, under decreasing oxygen partial pressure, a change in the primary crystallization products is observed, cuprates growing under high oxygen pressures whereas the 23X phase nucleates in oxygen deficient atmospheres. Therefore, it should be possible to minimize the primary nucleation of either of these phases by solidification under an appropriate low-oxygen-pressure atmosphere.

The results from these studies have been applied to the development of Bi-2212 current leads. In order to control the composition during solidification, a Sr-rich composition such as $Bi_2Sr_{2.15}Ca_{0.85}Cu_2O_x$ is used. This composition minimizes problems due to excessive CaO precipitation in the surface slag layer. The samples are then processed in an atmosphere with a reduced oxygen partial pressure in an effort to avoid primary precipitation of either the (Sr,Ca)CuO phases or the 23X phase. Large bars approximately 8 cm × 1.5 cm × 0.5 cm have been cast using these procedures. The properties of these bars have been evaluated by pulsed direct current transport measurements and magnetization hysteresis. The transport measurements have shown the sample have a critical current of 230A corresponding to a critical current density of 430 A/cm² at 77K in zero field, based on a 1 μv/cm criterion. Critical current densities estimated from magnetic hysteresis using Bean's model indicate a critical current density of over 65,000 A/cm² at 5K and 1 T and the J_c remains above 35,000 A/cm² to fields over 4 T. Based on these results, it is expected that a current lead bundle which could support up to 1000 A

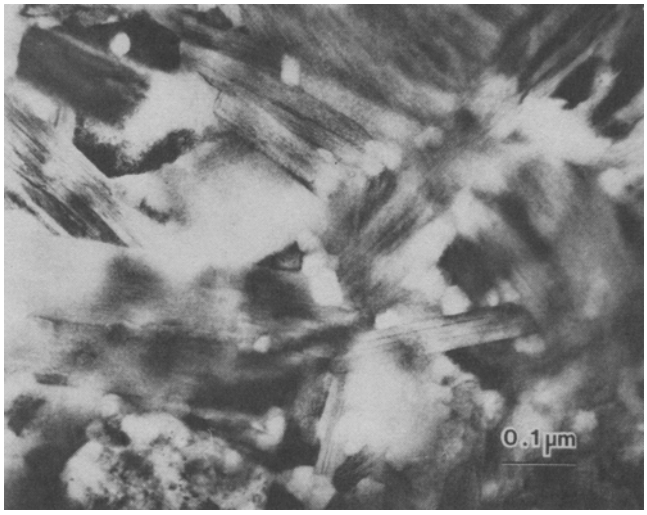

Fig. 7. Bright field transmission electron micrograph of a splat-quenched sample annealed at 750°C for 1 min.

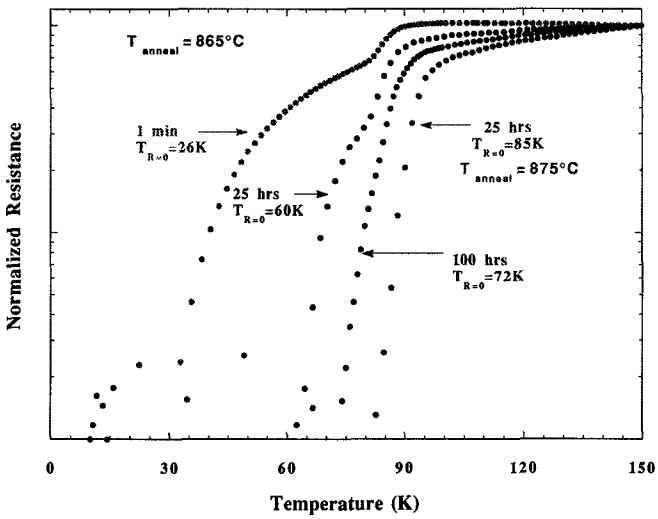

Fig. 8. Resistance vs temperature plots for samples annealed at 865 or 875°C for various times, as indicated. The resistance for each sample, plotted on a log scale, is normalized to the resistance at 150K.

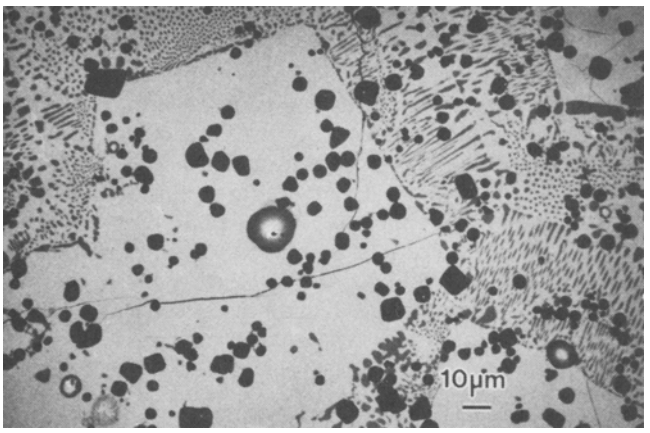

Fig. 9. Scanning electron back-scattered micrograph of a sample solidified in an argon atmosphere at a cooling rate of 10°C/min.

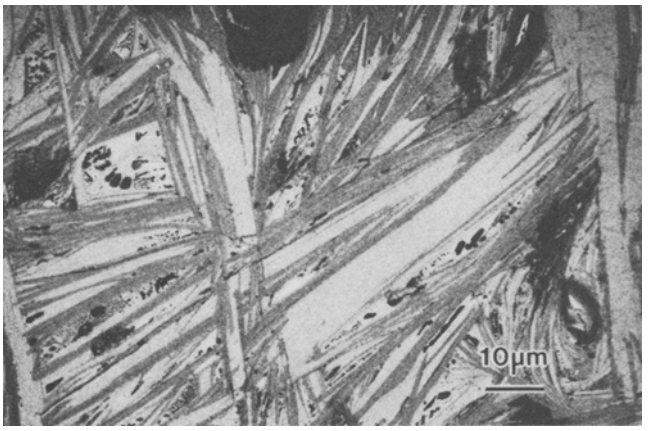

Fig. 10. Scanning electron back-scattered micrograph of a sample solidified in an oxygen atmosphere at a cooling rate of 10°C/min.

at 77K could be constructed from four or five of these bars.

CONCLUSIONS

The high-temperature mechanical deformation and consolidation of Bi-2212 have been studied and the effects on microstructure evaluated. It is found that high-temperature creep deformation occurs by diffusional creep at low stresses while dislocation creep and microcracking dominate at higher stresses. During consolidation by hot isostatic pressing, these same deformation mechanisms operate to densify the material. Once full densification is achieved, however, recovery processes dominate and the dislocation structure which contributes to enhanced flux pinning is annihilated resulting in reduced intragranular critical current densities. Solidification of Bi-2212 from the melt or crystallization from an amorphous glass are observed to be influenced strongly by oxygen deficiencies. During crystallization of the glass, the primary crystallization event occurs in an oxygen deficient environment due to limited diffusion of oxygen. As the annealing temperature is increased, however, partial melting of these phases results in enhanced oxygen mobility and rapid formation of the 2212 phase. During solidification, primary nucleation of cuprates followed by growth of the 2212 phase is observed in oxygen. In an argon atmosphere, primary 23X forms followed by eutectic solidification. By choosing an appropriate low-oxygen partial pressure, cast bars with high critical currents can be prepared by direct solidification. Critical currents of up to 230 A with a corresponding critical current density of 430 A/cm^2 have been measured for these samples.

ACKNOWLEDGMENTS

This work partially supported by the U.S. Department of Energy, divisions of Basic Energy Sciences-Materials Sciences, Conservation and Renewable Energy-Advanced Utility Concepts-Superconducting Technology Program, under contract No. W-31-109-ENG-38 and the National Science Foundation Office of Science and Technology Centers under contract DMR 91-20000. TH acknowledges support from the Argonne Division of Educational Programs.

REFERENCES

1. H. Maeda, T. Tanaka, M. Fukutomi and T. Asano, *Jpn. J. Appl. Phys.* 27, L209 (1988).
2. C. Michel, M. Hervieu, M.M. Borel, A. Grandin, F. Deslandes, J. Provost and B. Raveau, *Z. Phys. B* 68, 421 (1987).
3. D.H. Kim, K.E. Gray, R.T. Kampwirth, J.C. Smith, D.S. Richeson, T.J. Marks, J.H. Kang, J. Talvacchio and M. Eddy, *Physica C* 177, 431 (1991).
4. R.F. Geise, T.P. Sheahan, A.M. Wolsky and D.K. Sharma, *IEEE Trans.—Energy Conversion* 7, 589 (1992).
5. J.H. Kang, R.T. Kampwirth, K.E. Gray, S. Marsh and E.A. Huff, *Phys. Lett.* 128, 102 (1988).
6. T.A. Miller, S.C. Sanders, J.E. Ostenson, D.K. Finnemore, S.E. LeBeau and J. Righi, *Appl. Phys. Lett.* 56, 584 (1990).
7. T. Komatsu, R. Sato, C. Hirose, K. Matusita and T. Yamashita, *Jpn. J. Appl. Phys.* 27, L550 (1988).
8. M.R. DeGuire, N.P. Bansal and C.J. Kim, *J. Am. Ceram. Soc.* 73, 1165 (1990).
9. M. Yoshimura, T.H. Sung, Z. Nakagawa and T. Nakamura, *Jpn. J. Appl. Phys.* 27, L1877 (1988).
10. H. Takei, M. Koike, H. Takeya, K. Suzuki and M. Ichihara, *Jpn. J. Appl. Phys.* 28, L1193 (1989).
11. Y. Ibara, H. Nasu, T. Imura and Y. Osaka, *Jpn. J. Appl. Phys.* 28, L37 (1989).
12. K. Nassau, A.E. Miller, E.M. Gyorgy and T. Seigrist, *J. Mater. Res.* 4,1330 (1989).
13. A.S. Nash, P. Nash, H. Shi, R.B. Poeppel and K.C. Goretta, *Supercond. Sci. Technol.* 3, 556 (1990).
14. K. Ishizaki, M. Takata and H. Seino, *J. Mater. Sci. Lett.* 9, 16 (1990).
15. S.X. Dou, H. K. Liu, J. Wang and W.M. Bian, *Supercond. Sci. Technol.* 4, 21 (1991).
16. N. Murayama, E. Sudo, M. Awano, K. Kani and Y. Torii, *Jpn. J. Appl. Phys.* 27, L1856 (1988).
17. R. Yoshizaki, H. Ikeda, K. Yoshikawa and N. Tomita, *Jpn. J. Appl. Phys.* 29, L753 (1990).
18. C.-Y. Chu, J.L. Routbort, N. Chen, A.C. Biondo, D.S. Kupperman and K.C. Goretta, *Supercond. Sci. Technol.* 5, 306 (1992).
19. J.L. Routbort, K.C. Goretta, D.J. Miller, D.B. Kazelas, C. Clauss and A. Dominquez-Rodriguez, *J. Mater. Res.* 7, 2360 (1992).
20. D.J. Miller, S. Sengupta, J.D. Hettinger, D. Shi, K.E. Gray, A.S. Nash and K.C. Goretta, *Appl. Phys. Lett.* 61, 2823 (1992).
21. T.G. Holesinger, D.J. Miller and L.S. Chumbley, *J. Mater. Res.* 7, 1658 (1992).
22. M. Runder, J.L. Routbort, S.J. Rothman, K.C. Goretta, J.N. Mundy, X. Xu and J.E. Baker, *Phys. Rev. B* 45, 7375 (1992).